Assessment of the Current-Source, Full-Bridge Inverter as Power Supply for Ozone Generators With High Power Factor in a Single Stage

Mario Ponce-Silva, *Member, IEEE*, Juan Antonio Aqui, Víctor Hugo Olivares-Peregrino, *Member, IEEE*, and Marco Antonio Oliver-Salazar

***Abstract*—The arrangement of the full-bridge, current-source inverter as a power supply for ozone generators providing high power factor (PF) and high electrical efficiency in a single stage is the main contribution of this paper. The corresponding design, simulation, and experimental results are presented. Also, the use of the current-fed, full-bridge resonant inverter for PF correction in ozone generation applications is discussed. The proposed power supply consists of an ac supply, a single rectifier bridge, an input inductor to the inverter, four switches, an *LC* parallel resonant tank, a resonant transformer, and a set of ozone generating cells. Experimental results with the proposed topology provided 96% for PF, 91% for electrical efficiency, and ozone production of 614 mgO_3/min, satisfying the requirements of the standard 61000-3-2, class A.**

***Index Terms*—Current-fed full-bridge inverter, dielectric barrier discharge (DBD), power factor, ripple factor (RF).**

I. Introduction

THE ozone, considered as a powerful oxidant, is nowadays used in different applications such as; water purification, ozone therapy, odontology, air disinfection, pool cleaning, and different biomedical and cleaning applications [1]–[3]. The most common method used for ozone generation is the dielectric barrier discharge (DBD). This method consists of two parallel electrodes connected to an ac power supply separated by one or more layers of dielectric material [4]. Between the dielectric material and one of the electrodes air or oxygen is supplied in the presence of high voltage between the electrodes, allowing the dissociation of oxygen molecules to form ozone.

There are different topologies used as power supply for the DBD aimed to integrate long life, small size, weight, and reduced cost and able to provide the necessary voltage to start the discharge process. On the other hand, there are two main features to be considered when the power supply is designed for any type of load: electrical efficiency and power factor (PF).

Manuscript received October 21, 2015; revised December 15, 2015; accepted January 08, 2016. Date of publication January 22, 2016; date of current version July 08, 2016. This work was supported by the National Council of Science and Technology (Conacyt). Recommended for publication by Associate Editor Francisco J. Azcondo.

The authors are with the Centro Nacional de Investigación y Desarrollo Tecnológico (CENIDET), Tecnológico Nacional de México, Morelos 62490, México (e-mail: ponce@cenidet.edu.mx; juanantonio@cenidet.edu.mx; olivares@cenidet.edu.mx; moliver@cenidet.edu.mx).

Color versions of one or more of the figures in this paper are available online at http://ieeexplore.ieee.org.

Digital Object Identifier 10.1109/TPEL.2016.2520925

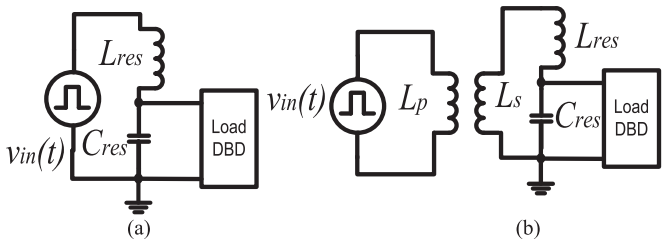

Fig. 1. Typical voltage-fed power supply for DBD.

The power factor is very important as it mainly influences the overall efficiency of the electric power system.

To correct the PF in single-phase systems, active and passive methods are reported in literature. Active methods, the ac–dc converters being the most common topologies, consist of resembling the input current waveform to a sinusoidal waveform in phase with the input voltage, [5]–[7], with the disadvantages of being complex, expensive, and producers of excessive electromagnetic interference (EMI).

Alternatively, passive solutions offer attractive benefits, including reliability, low cost, robust performance, and comparatively less EMI generation [8]. Examples of these solutions are *LC* filters, *LCD* rectifiers, and valley-fill circuits [9]–[11].

PF correction applied to DBD has been reported only in two cases [12], [13]. In [12], a high PF is achieved by an active method (boost converter). However, there is a compromise between the PF and the output power. In [13], a full-bridge inverter with PF 0.99 is presented where the PF is corrected by a passive method. However, the electrical efficiency is not cited.

Moreover, it is common to use resonant converters with voltage sources to feed the DBD [14]–[16]. Fig. 1(a) shows the basic configuration to elevate voltage using resonant converters. It is composed of a series resonant $L_{\rm res} - C_{\rm res}$ circuits and the voltage applied to the load is limited by the parasitic resistances of the elements. Furthermore, when the power is increased, it is necessary to increase the voltage in the DBD, and therefore, the need for a transformer, as is shown in Fig. 1(b). Due to the need of a high transformation ratio, the electrical efficiency suffers a reduction.

Alternatively, when the DBD is fed with an inverter current source, as shown in Fig. 2, the voltage across L_p is determined by the fundamental input current $i_{\rm in}$. The voltage across the primary winding of the transformer v_{L_p} is comparatively higher than the input voltage of the inverter voltage source topology

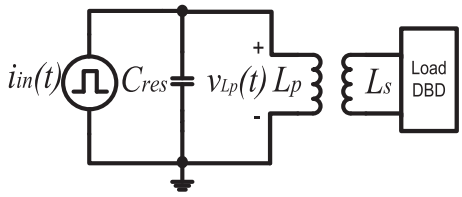

Fig. 2. Current-fed power supply for DBD.

[see Fig. 1(b)]. Therefore, the transformation ratio is smaller than that would be used in one conventional voltage source inverter with one similar transformer. Moreover, the inductor $L_{\rm res}$ is eliminated, but a bigger inductor is added to obtain the current source.

Feeding the DBD with a current-source inverter redeems a comparatively more stable performance as in the discharge stage the DBD emulates a capacitive behavior for which the current source provides a more precise control over the output voltage [17], [18]. So, in applications of DBD in lamps, surface treatment and ozone generation where the short circuit on the DBD load happens from time to time for the best performance of microdischarges generation are essential for the current-source resonant inverters because they have anti-short-circuit ability [19]. For the specific case of DBD lamps, as there exists a strong relation between the ultraviolet (UV) emission and the gas current, the use of a current supply to feed the different types of DBD is preferable [20].

Current-fed inverters applied to the DBD for ozone generation have been reported in [21]–[23]. Only [22] reports an achieved electrical efficiency of 76% without consideration of the PF correction stage. In [13], an inverter with high PF is presented without consideration of the electrical efficiency. Fig. 3 presents these three current-fed inverters reported in the literature.

For any one of the above inverters of Fig. 3 to be connected to the electrical network is becomes necessary the addition of a PF correction circuit as it is sketched in Fig. 4.

The main disadvantage of the current-fed inverters is the bulky inductor [$L_{\rm input}$ in Fig. 3(a)] in the input of the circuit; this inductor increases the weight and size of the power supply. Nevertheless, this disadvantage could be an advantage when this inductor is used instead of the PFC stage. Since such an inductor is cheaper, and if it substitutes the electrolytic capacitor, then the useful life of the power supply is increased.

This paper presents a power supply for ozone generation purposes based on a current-fed, full-bridge resonant inverter with an input inductor for PF correction in a single stage as it is depicted in Fig. 5.

The proposed topology does not require an additional stage for PF correction, and furthermore, an efficiency of 91% and a PF of 96% are obtained.

The structure of this paper is as follows: In Section II, the proposed inverter with the corresponding analysis and design methodology are described. Section III presents the experimental results, and Section IV compares these results with others reported in the literature. Finally, Section V presents the conclusions.

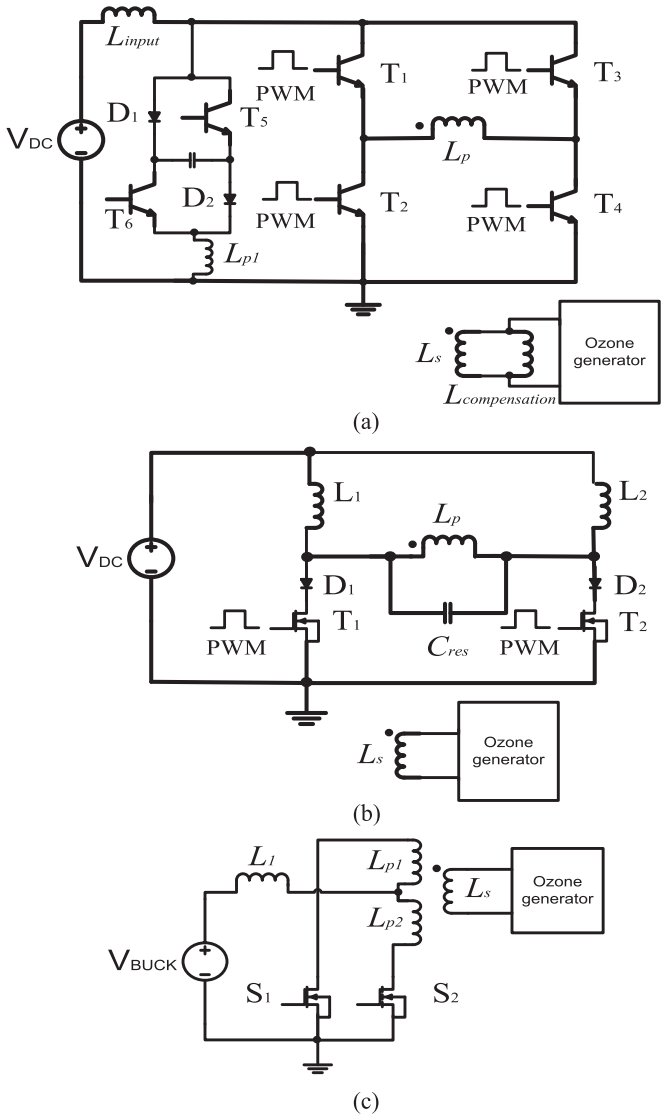

Fig. 3. Current-fed inverters for ozone generation: (a) inverter full bridge, (b) push–pull, and (c) buck and push–pull.

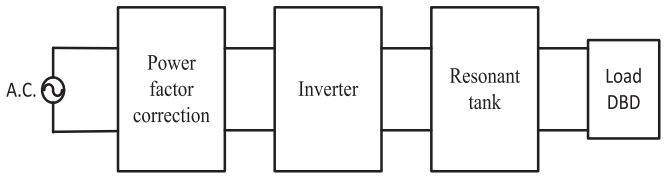

Fig. 4. Typical power supply

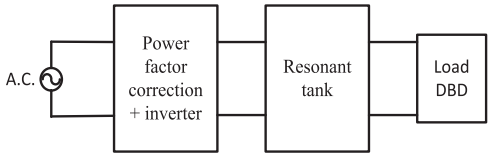

Fig. 5. Integrated power supply

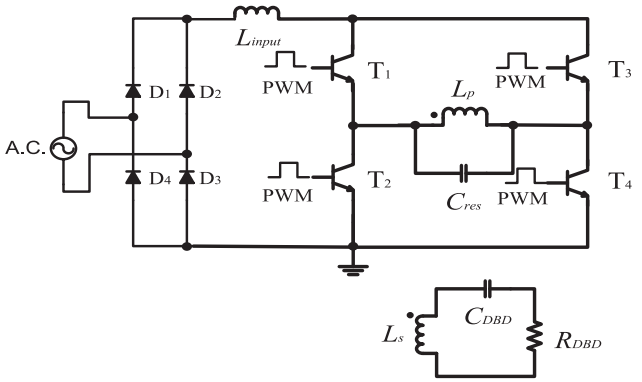

Fig. 6. Current source full-bridge inverter.

II. Proposed Power Supply

The main contribution of this paper is the use of an input inductor to passively correct the PF in current-source inverters. The proposed current-fed, full-bridge inverter is shown in Fig. 6. It includes four switches (T1–T4), $L_p - C_{\rm res}$ parallel resonant tank (where L_p is coupled to a secondary inductor L_s), and a set of ozone-generating cells represented by $R_{\rm DBD}$ and $C_{\rm DBD}$. There are several electrical models of DBD reported in the literature: a nonlineal model based in a diodes bridge [24], a lineal model based in a parallel circuit *RC* [25]–[27], and a lineal model based in a series circuit *RC* [28]–[31]. The nonlineal model based in a diode bridge is mainly applied to frequencies lower than 10 kHz, and the series *RC* model has been applied to fluorescent and excimer lamps. The parallel *RC* model has been widely applied to ozone chambers and works properly with symmetrical voltage waveforms with no dc component. For symmetrical voltage waveforms, both models are electrically equivalent. However, with nonsymmetrical waveforms that present a dc component, the dc component would be applied to the equivalent parallel resistance and it will contribute to generate the microdischarges that separate the oxygen molecules producing more ozone. This is wrong since the ozone generator has a dielectric in series with the ozone chamber, and this dielectric represents a capacitor in series with the ozone chamber. This capacitor avoids the dc voltage component be applied to the ozone chamber, and microdischarges cannot be produced by this component. Due to this reason, the series *RC* model of the ozone chamber is preferred and used in this paper.

For simplicity purposes, the full-bridge inverter is represented with an equivalent resistance *R*. The equivalent circuit is shown in Fig. 7(a) and consists of a filter $L_{\rm input}R$, and the input voltage and current waveforms with maximum current ripple in $L_{\rm input}$ is shown in Fig. 7(b). Progressively, the resonant tank in parallel connection with the DBD, fed by the current-source inverter, is analyzed. In all the analyses, the semiconductors and passive elements are considered as ideal.

A. Analysis of the $L_{\rm input}R$ Filter

Applying the Kirchhoff voltages law to Fig. 7, the following expression is obtained:

$$L\frac{di_L(t)}{dt} + Ri_L(t) = |V_p \sin\omega t|\,. \tag{1}$$

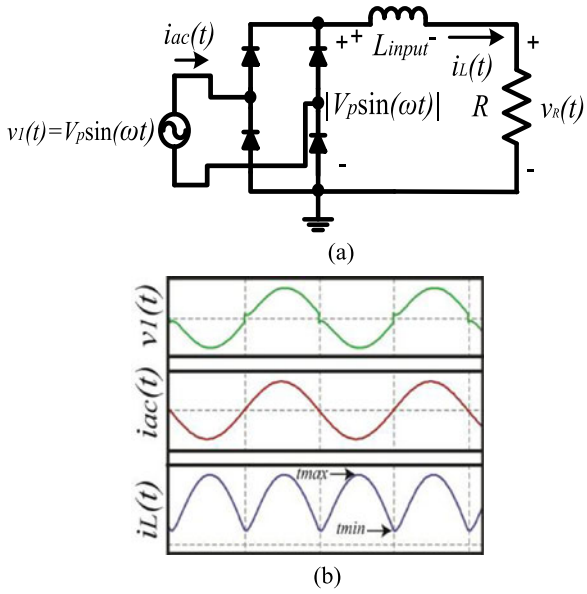

Fig. 7. (a) Equivalent circuit of the current-fed inverter and (b) theoretical input waveforms with current ripple of 90% in $L_{\rm input}$.

The solution in steady state of (1) is

$$i_L(t) = \begin{cases} \dfrac{V_p}{Z_e}\left[\sin(\omega t-\phi) + \dfrac{2\sin\phi}{1-e^{-\frac{\pi}{\omega\tau}}}e^{-\frac{t}{\tau}}\right], & 0 \le t \le \frac{\pi}{\omega} \\ \dfrac{V_p}{Z_e}\left[-\sin(\omega t-\phi) + \dfrac{2\sin\phi}{e^{-\frac{\pi}{\omega\tau}}\left(1-e^{-\frac{\pi}{\omega\tau}}\right)}e^{-\frac{t}{\tau}}\right], & \frac{\pi}{\omega} < t < \frac{2\pi}{\omega} \end{cases} \tag{2}$$

where the phase angle is

$$\phi = \tan^{-1}\left(\frac{\omega L_{\rm input}}{R}\right). \tag{3}$$

The equivalent impedance is given by

$$Z_e = \sqrt{R^2 + (\omega L_{\rm input})^2}. \tag{4}$$

The time constant τ is

$$\tau = \frac{L_{\rm input}}{R}. \tag{5}$$

B. Ripple Voltage (ΔV) and RF of Load Voltage (v_R).

The ripple voltage (ΔV) is the difference between the maximum value of the load voltage $v_R(t)$, i.e., $V_{\max}$, and the minimum value of $v_R(t)$, i.e., $V_{\min}$. Also, it is useful and common to relate ΔV with $V_{\max}$ to obtain a percentage figure. This relationship is the ripple factor (RF) as in [32] and is given by

$$\text{RF} = \frac{\Delta V}{V_{\max}} = \frac{V_{\max} - V_{\min}}{V_{\max}}100\%. \tag{6}$$

Also, RF is equal to the ripple current in the resistor ΔI, divided by the maximum current in *R* $I_{\max}$, as shown

$$RF = \frac{\Delta I}{I_{\max}} = \frac{I_{\max} - I_{\min}}{I_{\max}}100\% \tag{7}$$

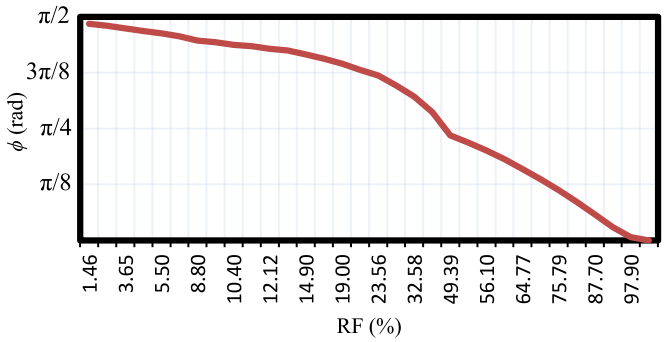

Fig. 8. Variation of RF (%) versus φ (rad).

where $I_{\min}$ is the minimum current in R.

$V_{\max}, V_{\min}, I_{\max}$, and $I_{\min}$ depend on $V_p, Z_e, \varphi, \tau, \omega$, and t. The specific time t at which $V_{\max}$ and $I_{\max}$ occur is $t_{\max}$, and when $V_{\min}$ and $I_{\min}$ occur is the time symbolized by $t_{\min}$. To obtain $t_{\max}$ and $t_{\min}$, (2) could be derived and equalized to zero. However, the result is not an analytic solution as it can be seen from (8)

$$t = \cos^{-1}\left\{\frac{\left[\left(2\sin\phi e^{-\frac{t}{\tau}}\right)/\left(\omega\tau\left(1-e^{-\frac{\pi}{\omega\tau}}\right)\right)\right]+\phi}{\omega}\right\}. \quad (8)$$

By numerically solving (8), it is possible to find $t_{\max}$, if the second derivative of (2), say i_s, is such that $i_s < 0$ and to obtain $t_{\min}$, provided $i_s > 0$. In such a way, the obtained times are substituted in (2) to obtain $I_{\max}$ and $I_{\min}$.

Since $i_L(t)$ is a periodical signal, $t_{\min}$ and $t_{\max}$ can be presented as angles (β for $t_{\max}$ and ζ for $t_{\min}$) and dividing these parameters by ω, one gets

$$t_{\max} = \frac{\beta}{\omega}, \qquad t_{\min} = \frac{\zeta}{\omega}. \quad (9)$$

Each RF value proposed for the $L_{\text{input}}R$ filter corresponds to specific values for the angles β and ζ. A set of values for these angles could be numerically evaluated for different values of RF, and with the collected values, it is possible to obtain the phase angle φ. Fig. 8 presents the variation of φ in terms of RF.

C. Evaluation of the Average Power Delivered by the Current Source

Since, the input current $|i_{\text{ac}(t)}| = |i_L(t)|$ during all the period, the root mean square (RMS) of $i_{\text{ac}}(t)$ is $I_{\text{ac rms}} = I_{L_{\text{rms}}}$

$$I_{L\text{rms}} = \sqrt{\frac{1}{T}\int_0^T i_L(t)^2 dt}$$
$$= \frac{V_p}{Z_e}\sqrt{\frac{1}{2}+\frac{\omega\tau}{2\pi}\left(\frac{2\sin\phi}{1-e^{-\frac{\pi}{\omega\tau}}}\right)^2\left(1-e^{-\frac{2\pi}{\omega\tau}}\right)}. \quad (10)$$

Solving for L_{input} from (3) and replacing it in (4), (5), and (10) give

$$I_{L_{\text{rms}}} = \frac{V_p}{R\sqrt{1+\tan^2\phi}} \times\sqrt{\frac{1}{2}+\frac{\tan\phi}{2\pi}\left(\frac{2\sin\phi}{1-e^{-\frac{\pi}{\tan\phi}}}\right)^2\left(1-e^{-\frac{2\pi}{\tan\phi}}\right)}. \quad (11)$$

From (11), the average power in the resistor R is

$$P_{\text{avg}} = I_{\text{rms}}^2 R = \frac{V_p^2}{R(1+\tan^2\phi)}\left(\frac{1}{2}+\frac{\tan\phi}{2\pi}\left(\frac{2\sin\phi}{1-e^{-\frac{\pi}{\tan\phi}}}\right)^2 \times\left(1-e^{-\frac{2\pi}{\tan\phi}}\right)\right). \quad (12)$$

D. $L_{\text{input}}R$ Filter Design

According to the previous analysis, it is possible to design a $L_{\text{input}}R$ filter. For example, for $V_p = 180$ V, $P_{\text{avg}} = 500$ W, and $f = 60$ Hz, the voltage ripple in R is proportional to the current ripple in R, so the RF is calculated using (7).

Fig. 8 shows the variation of the shift angle versus RF to calculate the rectifier inductor. In this paper, an RF = 90% is chosen. Considering the proposed parameters and ϕ, R is evaluated as

$$R = \frac{V_p^2}{P_{\text{avg}}(1+\tan^2\phi)}\left(\frac{1}{2}+\frac{\tan\phi}{2\pi}\left(\frac{2\sin\phi}{1-e^{-\frac{\pi}{\tan\phi}}}\right)^2 \times\left(1-e^{-\frac{2\pi}{\tan\phi}}\right)\right) = 30.1\ \Omega.$$

L_{input} is evaluated using (3) as

$$L_{\text{input}} = \frac{R\tan\phi}{\omega} = 11.25\,\text{mH}.$$

The PF is evaluated as

$$\text{PF} = \frac{(1/T)\int_0^T (v_1(t)i_{\text{ac}}(t))dt}{I_{\text{rms input}}V_{\text{rms input}}} \quad (13)$$

where $v_1(t)$ is the alternating input voltage, $i_{\text{ac}}(t)$ is the alternating input current, I_{rmsinput} is the rms input current, V_{rmsinput} is the rms input voltage, and T is the integration period.

From (13), PF is evaluated for each ripple factor (RF), resulting the graphic shown in Fig. 9.

For a value of RF = 90%, a value of PF = 98% corresponds. Moreover, the total harmonic distortion (THD) becomes

$$\text{THD} = \sqrt{\frac{1}{\text{PF}^2}-1} = 20.3\%.$$

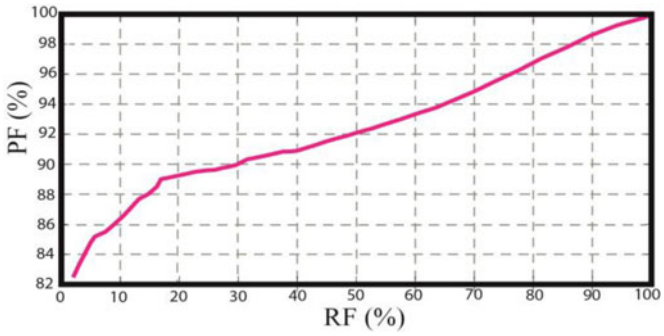

Fig. 9. Graphic of RF (%) versus PF.

E. Analysis of the Current-Source, Full-Bridge Inverter

The current-source, full-bridge inverter (CSFBI), shown in Fig. 6, can be simplified to the equivalent circuit presented in Fig. 10(a). In this equivalent circuit, the CSFBI is represented by a current square waveform [$i_{\rm in}(t)$] feeding a parallel resonant tank formed by L_p and $C_{\rm res}$. In this figure, the leakage inductances of the resonant transformer ($L_{\rm LP}$ and $L_{\rm LS}$) has been added. As can be seen in Fig. 10(a), the impedance of the inductance $L_{\rm LS}$ is in series with the impedance of $C_{\rm DBD}$, since the impedance of $L_{\rm LS}$ is very lower than the impedance of $C_{\rm DBD}$ then can be neglected or rested to the impedance of $C_{\rm DBD}$. On the other hand, the leakage inductance $L_{\rm LP}$ presents a voltage divider between $L_{\rm LP}$ and the magnetizing inductance L_P, since $XL_P \gg XL_{\rm LP}$, then this leakage inductance can be neglected too for this application.

The equivalent impedance of the CDBD and RDBD series model is

$$Z_e = \frac{R_{\rm DBD}}{1+\omega_0^2 R_{\rm DBD}^2 C_{\rm DBD}^2} - j\frac{\omega_0 R_{\rm DBD}^2 C_{\rm DBD}}{1+\omega_0^2 R_{\rm DBD}^2 C_{\rm DBD}^2}$$

$$\text{if} \quad R_{\rm DBD} >> \frac{1}{C_{\rm DBD}\omega_0}, \quad \text{then} \quad Z_e \approx \frac{1}{\omega_0^2 R_{\rm DBD} C_{\rm DBD}^2} - j\frac{1}{\omega_0 C_{\rm DBD}}.$$

Therefore, the $C_{\rm DBD}$ and $R_{\rm DBD}$ series model can be represented by a parallel equivalent circuit, as shown in Fig. 10(b), where $C_{{\rm DBD}p} = C_{\rm DBD}$ and $R_{{\rm DBD}p} = 1/\omega_0^2 R_{\rm DBD} C_{\rm DBD}^2$.

Fig. 10(c) shows $R_{{\rm DBD}p}$ and $C_{{\rm DBD}p}$ reflected on the inductor primary, where C_a and R_a represent, respectively, the capacitance and the resistance of $C_{{\rm DBD}p}$ and $R_{{\rm DBD}p}$ seen from the primary side of the transformer, $C_a = C_{{\rm DBD}p} n^2$ and $R_a = R_{{\rm DBD}p}/n^2$. Capacitors C_a and $C_{\rm res}$ can be represented by C_b, where $C_b = C_a + C_{\rm res}$, as shown in Fig. 10(d).

The equivalent circuit shown in Fig. 10(d) has been analyzed using the fundamental approximation and the phasorial representation and considering ideal elements. Consequently, the equivalent circuit with phasorial representation is presented in Fig. 11, where $I_{\rm in1}\angle 0$ is the fundamental input current phasor feeding the resonant tank, with $I_{\rm in1}$ being the maximum of the signal $i_{\rm in1}(t)$, and $I_{\rm out}\angle\theta$ is the output current phasor, with $I_{\rm out}$

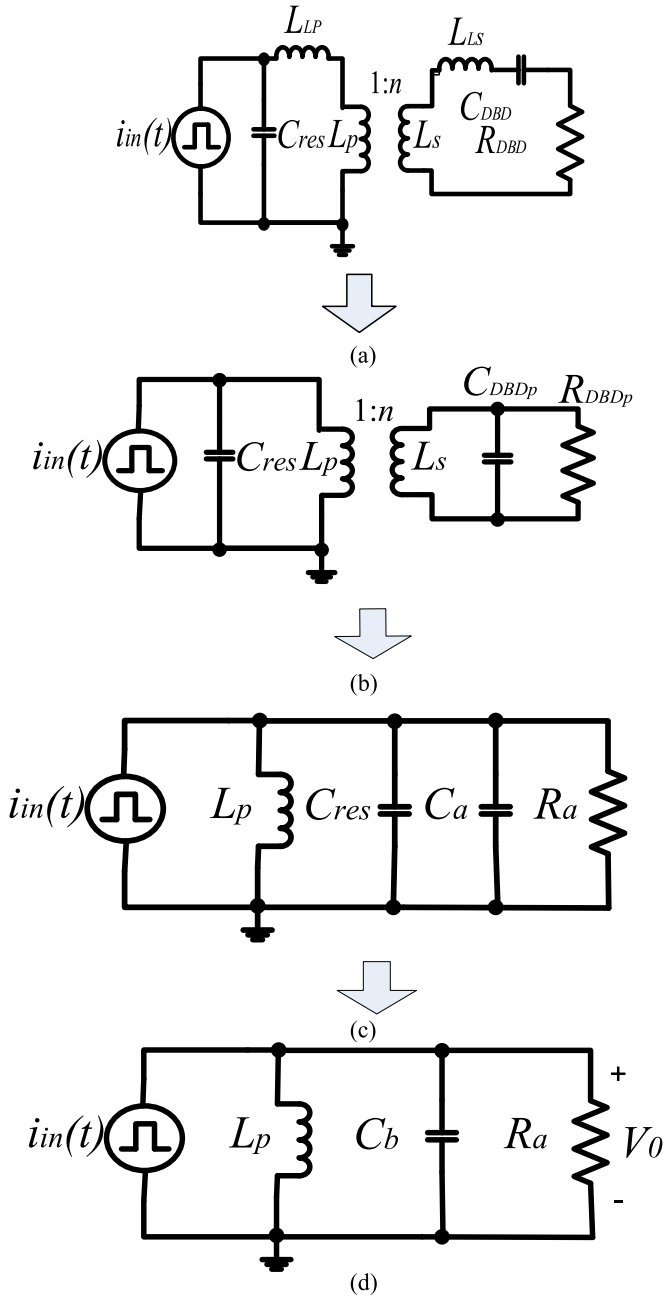

Fig. 10. Equivalent circuit of the current-fed inverter and DBD model.

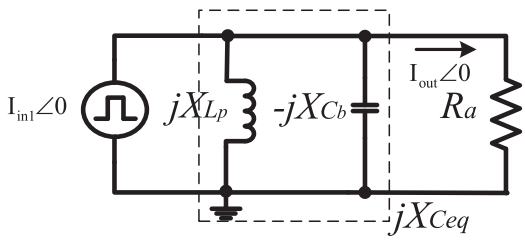

Fig. 11. Equivalent circuit represented by phasors.

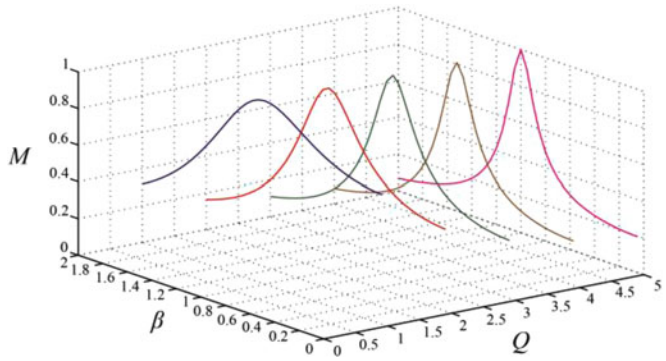

Fig. 12. Gain versus β and Q.

being the maximum of the signal $i_{\rm out}(t)$

$$\text{Also} \quad jX_{C_b} = 1/\omega C_b \quad \text{and} \quad jX_{L_p} = \omega L_p.$$

The equivalent reactance of the equivalent circuit is

$$X_{C_{\rm eq}} = \frac{-jX_{L_p}X_{C_b}}{X_{L_p} - X_{C_b}}. \tag{14}$$

The amplitude gain (M) is given by

$$|M| = \frac{|I_{\rm out}\angle 0|}{|I_{\rm in1}\angle 0|} = \frac{\left|X_{C_{\rm eq}}\right|}{\left|R_a + X_{C_{\rm eq}}\right|} = \frac{\left|-jX_{L_p}X_{C_b}\right|}{\left|(X_{L_p} - X_{C_b})(R_a - (jX_{L_p}X_{C_b})/(X_{L_p} - X_{C_b}))\right|} \tag{15}$$

which can be simplified to

$$|M| = \frac{1}{\sqrt{Q^2(1-\beta^2)^2 + 1}} \tag{16}$$

where Q is the quality factor, β is the ratio between ω_0 and ω_s, ω_0 is the angular resonant frequency, and ω_s is the angular frequency, and therefore

$$\beta = \frac{\omega_0}{\omega_s}, \quad \omega_0 = \frac{1}{\sqrt{L_p C_b}}, \quad \text{and} \quad Q = \frac{R_a}{X_{C_b}}$$

Based on (16) with different values for β and Q, the graphic shown in Fig. 12 has been obtained exhibiting only one point with unity gain ($M = 1$) when the topology is operated in resonance regardless of the value of Q. However, the choice of a high value for Q results in bigger size reactive components.

The average current $I_{\rm dc}$ in the inductor $L_{\rm input}$ (see Fig. 7) can be calculated as

$$I_{\rm dc} = \frac{1}{T}\int_0^T iL_{\rm input}(t)dt = \frac{2V_p}{\pi Z_e}(\cos\phi + \omega\tau\sin\phi). \tag{17}$$

By considering a duty cycle of $D = 50\%$ for the CSFBI, the input fundamental current $I_{\rm in1}$ is

$$I_{\rm in1} = \frac{4I_{\rm dc}}{\pi}. \tag{18}$$

TABLE I
DESIGN METHODOLOGY FOR THE CURRENT-FED INVERTER

Parameter	Equation	Calculated value
$i_{\rm DC}$	$\frac{2V_p}{\pi Z_e}(\cos\phi + \omega\tau\sin\phi)$	3.807 A
$i_{\rm in1}$	$\frac{4i_{\rm DC}}{\pi}$	4.84 A
V_0	$\frac{2P_{\rm out}}{i_{\rm in1}}$	206.61 V
R_a	$\frac{V_0^2}{2P_{\rm out}}$	42.68 Ω
C_b	$\frac{Q}{\omega_0 R_a}$	1.86 μF
L_p	$\frac{1}{\omega_0^2 C_b}$	135 μH
$R_{{\rm DBD}p}$	$\frac{1}{\omega_0^2 R_{\rm DBD} C_{\rm DBD}^2}$	230.27 Ω
n	$\sqrt{\frac{R_{{\rm DBD}p}}{R_a}}$	2.32
L_s	$L_p n^2$	13.58 mH
C_a	$C_{{\rm DBD}p} n^2$	53 nF
$C_{\rm res}$	$C_b - C_a$	1.80 μF

For ideal passive and semiconductor elements, the output voltage and the equivalent resistor can be calculated as

$$V_0 = \frac{2P_{\rm out}}{I_{\rm in1}} \quad \text{and} \quad R_a = \frac{V_0^2}{2P_{\rm out}}. \tag{19}$$

The resonant capacitor is determined by the quality factor Q, the angular resonant frequency ω_0, and the equivalent resistor R_a as

$$C_b = \frac{Q}{\omega_0 R_a}. \tag{20}$$

As the primary inductor is in resonant mode with $C_{\rm res}$, then

$$L_p = \frac{1}{\omega_0^2 C_b}. \tag{21}$$

As it was previously addressed, the primary and secondary inductors are coupled as

$$L_s = L_p n^2. \tag{22}$$

F. Design Methodology for the Current-Fed, Full-Bridge Inverter

Based on the performed analysis and the *LR* filter design, Table I presents a design methodology for the proposed values. The specifications for this design are as follows: $P_{\rm out} = 500$ W, $f_0 = 10$ kHz, $Q = 5$, and $V_p = 180$ V. The previously calculated filter provided the values of $L_{\rm input} = 11.25$ mH, $\varphi = 0.1399$ rad, and $R = 30.1$ Ω.

The considered load for the proposed circuit is the set of ozone generating cells shown in Fig. 13(a), and it is based on the parallel-plate configuration. The design consists of two stainless steel plates covered by resin and fiberglass; each plate is adhered to a heatsink where a high voltage is applied. Two connectors were also added for the oxygen input and ozone output. One of these ozone generator cells is shown in Fig. 13(b). Each

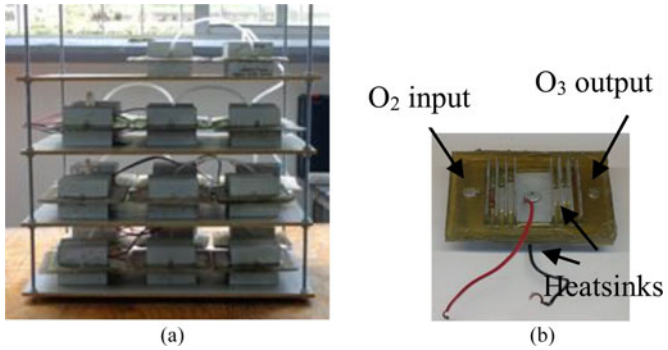

Fig. 13. Designed ozone generating cells. (a) Set of ozone-generating cells. (b) Single ozone-generating cell

cell demands a power of 25 W, and 20 cells were connected to provide the required power.

The cells were characterized using the model described in [28], and the obtained values were $R_{\mathrm{DBD}} = 11$ kΩ and $C_{\mathrm{DBD}} = 10$ nF. The switching frequency of 10 kHz was chosen to test the design methodology and the current-fed inverter experimentally. Due this ozone-generating cells have not forced ventilation, the used ozone-generating cells produces more ozone for frequencies below of 20 kHz. For highest frequency, the temperature in ozone camera is increased to 50 °C; in this temperature, the ozone produced is converted to oxygen [33].

The next table presents each parameter, the corresponding equation, and the calculated value.

III. Experimental Results

Based on the design methodology shown in Table I and the designed filter L_{input}, a prototype was developed to obtain experimental parameter values.

The CSFBI electrical diagram and the implemented CSFBI prototype are shown in Fig. 14(a) and (d), respectively. The switching pulsewidth-modulated (PWM) control signals are generated with the TL494 circuit, and a totem pole driver circuit has been implemented using the BD135 and BD136 transistors. Isolation of the control stage from the power stage was achieved with pulse transformers. The inverter switches were IRG4PH40U IGBTs. The selected rectifier diodes were MUR860. Signal measurements were obtained with the Tektronix DPO5054 oscilloscope using the P5210A, TCP0030, and P2220 probes. The ozone concentration was measured with the 450H model API ozone monitor.

To feed the ozone generator, an oxygen flow of 0.7 LPM (liters per minute) was injected. The design of the input inductor and the transformer was based on the geometrical constant Kg. The leakage inductance in high-voltage transformers is usually very large, so the transformer used in this paper was wound in multiple interleaving of primary and secondary sections to improve the coupling and to reduce the leakage inductance. If this inductance is very large, it will cause trouble in tuning in the resonance frequency and, therefore, was proposed to decrease it (see Table II).

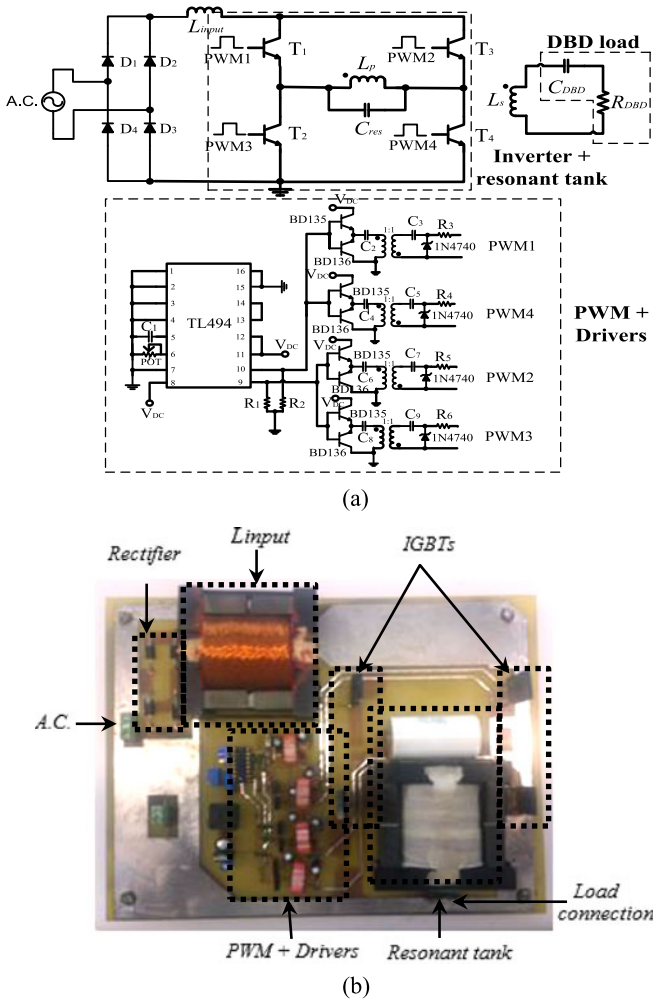

Fig. 14. (a) CSFBI electrical diagram and (b) CSFBI implemented.

Fig. 15(a) shows the current (upper trace) and voltage (lower trace) waveforms measured on the set of 20 cells. Fig. 15(b) shows the current (upper trace) and the voltage (lower trace) waveforms obtained by PSPICE simulations. As it can be seen, the experimentally obtained voltage shows a peak of 3.7 kV and the same voltage in simulation is 3.67 kV. By considering the component tolerances, these values are very close. A major difference can be appreciated in the current waveforms due the presence of microdischarges in the DBD.

The average power demand in the set of 20 cells is 530 W, slightly higher than the expected value as the ozone-generating cells demand more current than expected with the used model for the DBD represented by R_{DBD} and C_{DBD}.

Fig. 16 shows the variation of electrical efficiency versus normalized input voltage of the designed power supply. The efficiency level varies from 46% to 91%; low efficiency levels are due to the variation of the resistive and capacitive values (R_{DBD} and C_{DBD}) as those values vary with the output power delivered to the DBD. These variations, mainly due to R_{DBD}, modify the resonant tank operation to the out-of-resonance mode, producing an increase in the switching losses. However, it can be seen

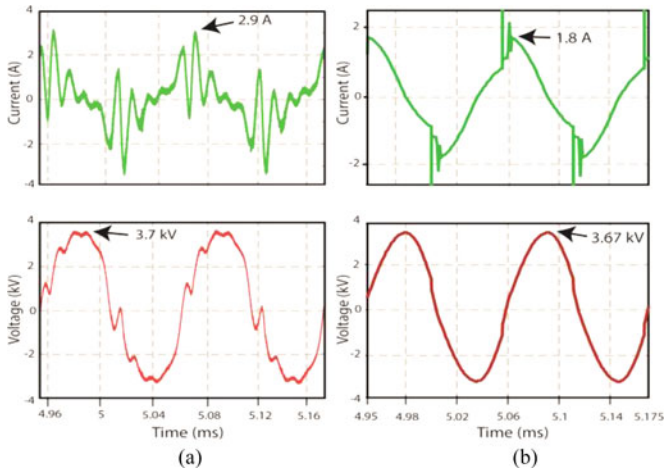

Fig. 15. (Top) Current and (bottom) voltage waveforms in ozone-generating cells: (a) experimental and (b) simulated.

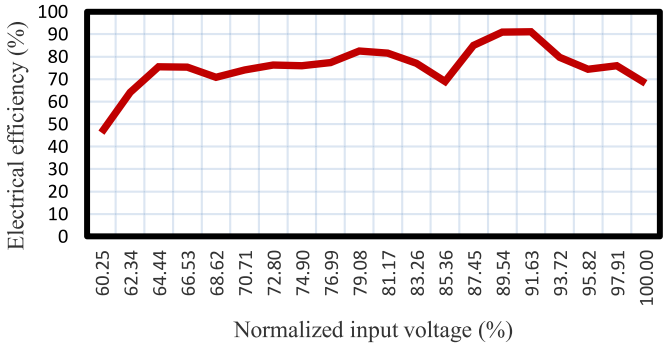

Fig. 16. Normalized input voltage versus efficiency.

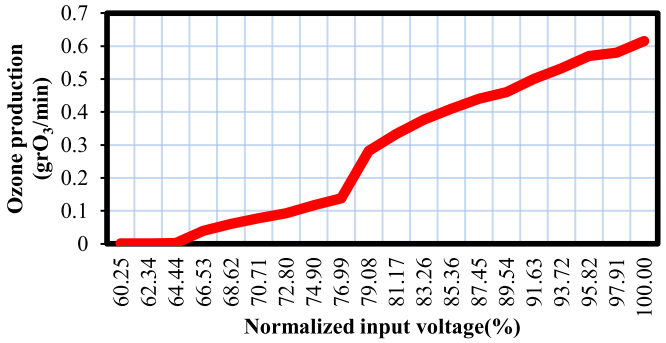

Fig. 17. Normalized input voltage versus ozone production.

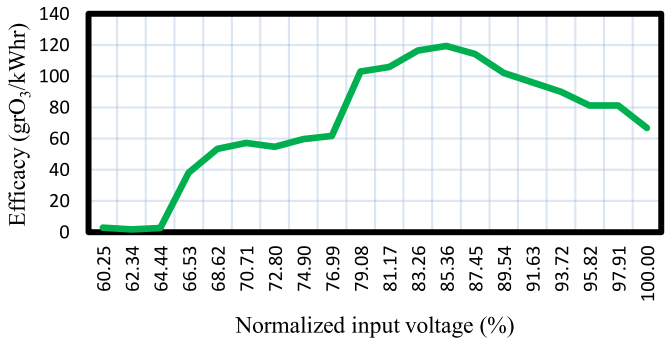

Fig. 18. Normalized input voltage versus efficacy.

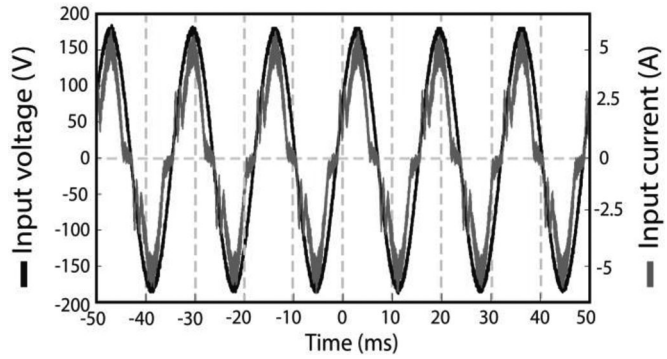

Fig. 19. Input voltage and current waveforms.

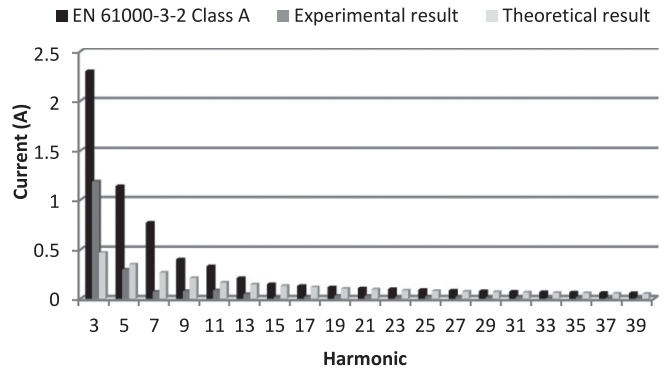

Fig. 20. Comparative graphic of harmonic content among the standard 61000-3-2 class A, experimental results, and simulated results.

that the efficiency remains above 70% for a wide range of input voltage values.

Fig. 17 presents a graphic of the ozone production variation versus the normalized input voltage for a constant oxygen flow of 0.7 LPM, reaching a maximum production of 0.614 grO_3/min.

Fig. 18 shows the variation of the efficacy of the ozone production (grO_3/kWh) versus the normalized input voltage. The maximum obtained efficacy is 119.28 grO_3/kWh, presenting a decrease in levels of the normalized input voltage of 85%–100% as the ozone production is less in this range.

Fig. 19 shows the input voltage and the current waveforms obtained under the nominal operation conditions in the prototype. As it can be seen, both waveforms present the same phase, the current waveform being almost sinusoidal, and therefore, the obtained PF is 96% with a THD of 30%.

Fig. 20 presents a comparative graphic of the harmonic amplitudes regarding the standard 61000-3-2 Class A. The figure shows the measured harmonics compared to the harmonics obtained by PSPICE simulations and the limits of the standard. As it can be appreciated in this comparison, the inductor of the current-source inverter (L_{input}) attenuates the harmonics in a considerable way, providing a high PF and complying with

TABLE II
POWER SUPPLIES APPLIED TO THE DBD IN OZONE GENERATION

Reference	Configuration	Power (W)	Electrical Efficiency (%)	Ozone Production (grO_3/min)
[22]	Inverter push–pull	28	76	–
[23]	Current-fed push–pull	100	–	0.2
[34]	Based on Class-E switching amplifier	10	91	–
[35]	Full-bridge inverter with *LCL* resonant tank.	8	92	0.12
[36]	Based on piezoelectric transformer.	6.2	95	0.0025
[37]	*LC* resonant half bridge	8	95	0.0095
This paper	Full-bridge resonant inverter	551	91	0.614

the requirements of the standard 61000-3-2 Class A in a single stage.

IV. COMPARISON WITH OTHERS WORKS

Table II lists some power supplies applied to the DBD for ozone generation, where the power, electrical efficiency, and ozone production are presented. It is clear that none of these references include the PF correction stage, and therefore, the electrical efficiency provided by the proposed topology is 91%, with a maximum ozone production of 614 mgO_3/min and a PF of 96%.

V. CONCLUSION

The main contribution of this paper is the use of the inductor in the CSFBI as a PF corrector in a single stage. The CSFBI uses a parallel resonant tank in a single-stage operation, allowing a considerable increment in efficiency up to a maximum of 91% with a PF of 96% and THD = 30% operating in a maximum power of 551 W. The ozone production was 0.614 grO3/min with an oxygen inflow of 0.7 LPM. The oxygen flow was low due the limitations of the available ozone monitor.

Among other advantages, the proposed topology complies with the requirements of the standard 61000-3-2 class A. Furthermore, it can be used in others applications of DBD, such as: plasma generation and any other capacitive load, it has minimal number of components by the single stage operation and low cost. The nonuse of electrolytic capacitors increases its lifetime.

REFERENCES

[1] V. Bocci, "Biological and clinical effects of ozone. Has ozone therapy a future in medicine?" *Br. J. Biomed. Sci.*, vol. 56, no. 4, pp. 270–279, 1999.

[2] M. Golkowski, C. Golkowski, J. Leszczynski, S. R. Plimpton, P. Maslowski, A. Foltynowicz, J. Jun, B. McCollister, "Hydrogen-peroxide-enhanced nonthermal plasma effluent for biomedical applications" *IEEE Trans. Plasma Sci.*, vol. 40, no. 8, pp. 1984–1991, Aug. 2012.

[3] Y. Song, D. Liu, Q. Lu, Y. Xia, R. Zhou, D. Yang, L. Ji, and W. Wang, "An atmospheric-pressure large-area diffuse surface dielectric barrier discharge used for disinfection application," *IEEE Trans. Plasma Sci.*, vol. 43, no. 3, pp. 821–827, Mar. 2015.

[4] L. Zhong-wei, L. Sen, C. Qiang, W. Zheng-duo, Y. Li-zhen, and L. Bin, "The spatiotemporal pattern formed in an atmospheric-pressure radio-frequency dielectric-barrier-discharge oxygen plasma," *IEEE Trans. Plasma Sci.*, vol. 39, no. 11, pp. 2130–2131, Nov. 2011.

[5] A. R. Prasad, P. D. Ziogas, and S. Manias, "A new active power factor correction method for single-phase buck-boost AC–DC converter," in *Proc. 7th Annu. Appl. Power Electron. Conf. Expo.*, 1992, pp. 814–820.

[6] S. Umesh, L. Venkatesha, and A. Usha, "Active power factor correction technique for single phase full bridge rectifier," in *Proc. 2014 Int. Conf. Adv. Energy Convers. Technol.*, pp. 130–135.

[7] X.-J. Yang, H. Wang, X.-H. Yang, H.-G. Lei, and H. Guan, "Theoretic analysis and experimental study of a novel bridgeless partial active PFC," in *Proc. Int. Conf. Elect. Machines Syst.*, 2008, pp. 1179–1184.

[8] W. M. Lin, M. M. Hernando, A. Fernandez, J. Sebastian, and P. J. Villegas, "A new topology for passive PFC circuit design to allow AC-to-DC converters to comply with the new version of IEC1000-3-2 regulations," in *Proc. IEEE 33rd Annu. Power Electron. Spec. Conf.*, 2002, pp. 2050–2055.

[9] C. Fărcas, D. Petreus, E. Simion, N. Palaghita, and Z. Juhos, "A novel topology based on forward converter with passive power factor correction," in *Proc. 29th Int. Spring Semin. Electron. Technol.*, 2006, pp. 268–272.

[10] J. Lam and P. K. Jain, "A simple single switch electronic ballast for compact fluorescent lamps with passive power factor correction (PFC) and soft switching capability," in *Proc. 38th Annu. Conf. IEEE Ind. Electron. Soc.*, 2012, pp. 4503–4508.

[11] J. C. W. Lam and P. K. Jain, "A modified valley fill electronic ballast having a current source resonant inverter with improved line-current total harmonic distortion (THD), high power factor, and low lamp crest factor," *IEEE Trans. Ind. Electron.*, vol. 55, no. 3, pp. 1147–1159, Mar. 2008.

[12] M. T. Tsai and C. L. Chu, "Power control strategies evaluation of a series resonant inverter for atmosphere plasma applications," in *Proc. IEEE Int. Symp. Ind. Electron.*, 2009, pp. 632–637.

[13] M. Akbari, V. Zahedzadeh, S. Shirmohammadzadeh, J. Chitsaz, and M. Chitsaz, "Efficient ozone generator using full-bridge inverter and its performance evaluations," in *Proc. 5th Int. Conf. Power Electron. Drive Syst.*, 2003, vol. 2, pp. 1182–1187.

[14] D. T. Rodrigues and J. A. Pomilio, "Resonant high-voltage supply for multiple paralleled loads with parameter equalization," in *Proc. 2011 Brazilian Power Electron. Conf.*, pp. 390–396.

[15] M. Meisser, R. Kling, and W. Heering, "Universal resonant topology for high frequency pulsed operation of dielectric barrier discharge light sources," in *Proc. 2011 26th Annu. IEEE Appl. Power Electron. Conf. Expo.*, pp. 1180–1187.

[16] P. Hothongkham and V. Kinnares, "High-voltage high-frequency power supply using a phase-shifted PWM full bridge inverter fed ozone generator with constant applied electrode voltage," in *Proc. 2010 Int. Power Electron. Conf.*, pp. 1560–1567.

[17] J. M. Alonso, J. Garcia, A. J. Calleja, J. Ribas, and J. Cardesin, "Analysis, design, and experimentation of a high-voltage power supply for ozone generation based on current-fed parallel-resonant push-pull inverter," *IEEE Trans. Ind. Appl.*, vol. 41, no. 5, pp. 1364–1372, Sep.–Oct. 2005.

[18] R. Diez, H. Piquet, D. Florez, and X. Bonnin, "Current-mode approach in power supplies for DBD excilamps: Review of 4 topologies," *IEEE Trans. Plasma Sci.*, vol. 43, no. 1, pp. 452–460, Jan. 2015.

[19] C. Lei, G. Tangtang, L. Jun, Z. Chi, D. Yan, and H. Xiangning, "Analysis and design of a current-source CLCC resonant converter for DBD applications," *IEEE Trans. Power Electron.*, vol. 29, no. 4, pp. 1610–1621, Apr. 2014.

[20] R. Diez, H. Piquet, S. Bhosle, and J. M. Blaquiere, "Current mode converter for dielectric barrier discharge lamp," in *Proc. IEEE Power Electron. Spec. Conf.*, 2008, pp. 2485–2491.

[21] Y. L. Feng, Y. Konishi, S. P. Wang, Y. X. Wang, E. H. Chu, O. Koudriavtsev, and M. Nakaoka, "Next generation current-source soft-switched PDM and PWM hybrid mode inverter for silent discharge ozone generating tube drive," in *Proc. 3rd Int. Power Electron. Motion Control Conf.*, 2000, vol. 1, pp. 312–317.

[22] J. M. Alonso, J. Cardesin, J. A. Martin-Ramos, J. Garcia, and M. Rico-Secades, "Using current-fed parallel-resonant inverters for electrodischarge applications: A case of study," in *Proc. 19th Annu. IEEE Appl. Power Electron. Conf. Expo.*, 2004, vol. 1, pp. 109–115.

[23] C. Ordiz, J. M. J. Alonso, M. A. D. Costa, J. Ribas, and A. J. Calleja, "Development of a high-voltage closed-loop power supply for ozone generation," in *Proc. 23rd Annu. IEEE Appl. Power Electron. Conf. Expo.*, 2008, pp. 1861–1867.
[24] J. M. Alonso, M. Valdés, A. J. Calleja, J. Ribas, and J. Losada, "High frequency testing and modeling of silent discharge ozone generators," *Ozone: Science & Engineering*, vol. 25, pp. 363–376, 2003
[25] J. M. Alonso, M. Valdés, A. J. Calleja, J. Ribas, and J. Losada, "High frequency testing and modeling of silent discharge ozone generators," *BOSE*, vol. 25, pp. 363–376, 2003.
[26] M. Amjad, Z. Salam, M. Facta, and K. Ishaque, "A simple and effective method to estimate the model parameters of dielectric barrier discharge ozone chamber," *IEEE Trans. Instrum. Meas.*, vol. 61, no. 6, pp. 1676–1683, Jun. 2012.
[27] V. Kinnares and P. Hothongkham, "Circuit analysis and modeling of a phase-shifted pulsewidth modulation full-bridge-inverter-fed ozone generator with constant applied electrode voltage," *IEEE Trans. Power Electron.*, vol. 25, no. 7, pp. 1739–1752, Jul. 2010.
[28] V. H. Olivares, M. Ponce-Silva, R. Osorio, and M. Juarez, "DBD modeling as a function of waveforms slope," in *Proc. IEEE Power Electron. Spec. Conf.,* 2007, pp. 1417–1422.
[29] U. N. Pal, A. K. Sharma, J. S. Soni, K. Sonu, H. Khatun, M. Kumar, B. L. Meena, M. S. Tyagi, B. J. Lee, M. Iberler, J. Jacoby, and K. Frank, "Electrical modelling approach for discharge analysis of a coaxial DBD tube filled with argon," *J. Phys. D Appl. Phys.*, vol. 42, p. 045213, 2009.
[30] H. Piquet, R. Díez, J.-M. Blaquière, S. Bhosle, and N. Roux, "DBD lamp converter design using an electrical model of the load," *Math. Comput. Simul.*, vol. 81, pp. 420–432, 2010.
[31] R. Valdivia-Barrientos, J. Pacheco-Sotelo, M. Pacheco-Pacheco, J. S. Benítez-Read, and R. López-Callejas, "Analysis and electrical modelling of a cylindrical DBD configuration at different operating frequencies," *Plasma Sources Sci. Technol.*, vol. 15, p. 237, 2006.
[32] M. Rashid, *Microelectronic Circuits: Analysis and Design. Cengage Learning*, USA, 2010.
[33] C. Gottschalk, J. A. Libra, and A. Saupe, *Ozonation of Water and Waste Water: A Practical Guide to Understanding Ozone and Its Applications*. Hoboken, NJ, USA: Wiley, 2009.
[34] R. A. Chinga, L. Jenshan, and S. Roy, "Self-tuning high-voltage high-frequency switching power amplifier for atmospheric-based plasma sterilization," *IEEE Trans. Plasma Sci.*, vol. 42, no. 7, pp. 1861–1869, Jul. 2014.
[35] M. Amjad, Z. Salam, M. Facta, and S. Mekhilef, "Analysis and implementation of transformerless LCL resonant power supply for ozone generation," *IEEE Trans. Power Electron.*, vol. 28, no. 2, pp. 650–660, Feb. 2013.
[36] J. M. Alonso, C. Ordiz, M. A. Dalla Costa, J. Ribas, and J. Cardesin, "High-voltage power supply for ozone generation based on piezoelectric transformer," *IEEE Trans. Ind. Appl.*, vol. 45, no. 4, pp. 1513–1523, Jul.–Aug. 2009.
[37] M. Amjad and Z. Salam, "Design and implementation of a high-frequency LC-based half-bridge resonant converter for dielectric barrier discharge ozone generator," *IET Power Electron.*, vol. 7, pp. 2403–2411, 2014.

Mario Ponce-Silva (S'94–A'00–M'01) was born in San Luis Potosi, Mexico, on May 24, 1970. He received the B.Eng. degree in electrical engineering from the San Luis Potosi Autonomous University, San Luis Potosi, in 1994, and the M.Sc. and Ph.D. degrees from Centro Nacional de Investigación y Desarrollo Tecnológico (CENIDET), Moreloss, Mexico, 1996 and 1999, respectively.

Since March 1999, he has been a Full-Time Professor and Researcher at CENIDET. His current research interests include electronic ballast for discharge lamps, power factor correction, soft switching techniques, resonant converters, and power supplies for ozone generators. He has authored or coauthored several papers in journals, magazines, and conferences.

Dr. Ponce-Silva is the AE of the IEEE TRANSACTIONS ON POWER ELECTRONICS. He was a Reviewer of the IEEE TRANSACTIONS ON POWER ELECTRONICS, the IEEE TRANSACTIONS ON INDUSTRIAL ELECTRONICS, and the IEEE TRANSACTIONS ON INDUSTRY APPLICATIONS.

Juan Antonio Aqui was born in Sinaloa, Mexico. He received the Electronic Engineering degree from the Los Mochis Institute of Technology (ITLM), Sinaloa, in 2009, the M.S. degree in electronic engineering from the National Center for Research and Technological Development [Centro Nacional de Investigación y Desarrollo Tecnológico (CENIDET)], Moreloss, Mexico, in 2011, where he is currently working toward the Ph.D. degree in electronic engineering

His current research interests include power electronic converters for DBD and lighting applications.

Víctor Hugo Olivares-Peregrino (S'06–M'09) was born in Zacapu, Michoacán, Mexico, on January 26, 1968. He received the bacehlor's degree in industrial electronics from the Technological Institute of San Luis Potosi, San Luis Potosi, Mexico, in 1993, the M.Sc. and Ph.D. degrees from the Centro Nacional de Investigación y Desarrollo Tecnológico (CENIDET), Moreloss, Mexico, in 1996 and 2008, respectively.

Since February 2011, he has been the Director at CENIDET and an Associate Professor and Researcher at the National Technological of Mexico (TecNM), Cuauhtemoc, Mexico, since September 1996. His current research interests include electronic ballast for discharge lamps, power factor correction, and power supplies for ozone generators by dielectric barrier discharge (DBD). He has authored or coauthored several papers in journals, magazines, and conferences.

Marco Antonio Oliver-Salazar received the Electromechanical Engineering degree from the Universidad Anahuac, Mexico, Mexico, in 1985, the M.Sc. degree in control and information technology from the University of Manchester Institute of Science and Technology, Manchester, U.K., in 1989, and the Ph.D. degree in control engineering from the University of Sheffield, Sheffield, U.K., in 1994.

From 1985 to 1996, he was as a Researcher at the Instituto de Investigaciones Electricas, Cuernavaca, Mexico. In 1996, he joined the Electronics Department and the Mechatronics Department as a Lecturer–Researcher at the Centro Nacional de Investigacion y Desarrollo Tecnologico, Cuernavaca. He is the author of several technical papers in international conferences and journals and has headed different research projects. His current research interests include digital signal processing and nonlinear control applied to power electronics, robotics and mechatronic systems, specially in the design and control of robotic hands, human rehabilitation systems, power electronic converters, and photovoltaic systems.